

Adsorption properties of BSA and DsRed proteins deposited on thin SiO2 layers: optically non-absorbing versus absorbing proteins

Adriana Scarangella, Marvine Soumbo, Christina Villeneuve-Faure, Adnen Mlayah, Caroline Bonafos, Marie-Carmen Monje, Christine Roques, Kremena Makasheva

▶ **To cite this version:**

Adriana Scarangella, Marvine Soumbo, Christina Villeneuve-Faure, Adnen Mlayah, Caroline Bonafos, et al.. Adsorption properties of BSA and DsRed proteins deposited on thin SiO2 layers: optically non-absorbing versus absorbing proteins. Nanotechnology, 2018, 29 (11), pp.115101. 10.1088/1361-6528/aaa68b . hal-01988678

HAL Id: hal-01988678
https://hal.science/hal-01988678

Submitted on 20 May 2019

HAL is a multi-disciplinary open access archive for the deposit and dissemination of scientific research documents, whether they are published or not. The documents may come from teaching and research institutions in France or abroad, or from public or private research centers.

L'archive ouverte pluridisciplinaire **HAL**, est destinée au dépôt et à la diffusion de documents scientifiques de niveau recherche, publiés ou non, émanant des établissements d'enseignement et de recherche français ou étrangers, des laboratoires publics ou privés.



Open Archive Toulouse Archive Ouverte (OATAO)

OATAO is an open access repository that collects the work of some Toulouse researchers and makes it freely available over the web where possible.

This is an author's version published in: http://oatao.univ-toulouse.fr/21170

Official URL: https://doi.org/10.1088/1361-6528/aaa68b

To cite this version:

Scarangella, Adriana and Soumbo, Marvine and Villeneuve-Faure, Christina and Mlayah, A and Bonafos, Caroline and Monje, Marie-Carmen and Roques, Christine and Makasheva, Kremena Adsorption properties of BSA and DsRed proteins deposited on thin SiO2 layers: optically non-absorbing versus absorbing proteins. (2018) Nanotechnology, 29 (11). 1-15. ISSN 0957-4484

Any correspondence concerning this service should be sent to the repository administrator:

tech-oatao@listes-diff.inp-toulouse.fr

https://doi.org/10.1088/1361-6528/aaa68b

Adsorption properties of BSA and DsRed proteins deposited on thin SiO_2 layers: optically non-absorbing versus absorbing proteins

A Scarangella[1,2,3], M Soumbo[1,4], C Villeneuve-Faure[1], A Mlayah[2], C Bonafos[2], M-C Monje[4], C Roques[4] and K Makasheva[1]

[1] LAPLACE, Université de Toulouse, CNRS, UPS, INPT, 118 route de Narbonne, F-31062, Toulouse, France

[2] CEMES-CNRS, Université de Toulouse, 29 rue Jeanne Marvig, BP 94347, F-31055, Toulouse, France
[3] FERMaT, Université de Toulouse, CNRS, UPS, INPT, INSA, Toulouse, France
[4] LGC, Université de Toulouse, CNRS, UPS, INPT, 35 chemin des maraîchers, F-31062, Toulouse, France

E-mail: kremena.makasheva@laplace.univ-tlse.fr

Abstract

Protein adsorption on solid surfaces is of interest for many industrial and biomedical applications, where it represents the conditioning step for micro-organism adhesion and biofilm formation. To understand the driving forces of such an interaction we focus in this paper on the investigation of the adsorption of bovine serum albumin (BSA) (optically non-absorbing, model protein) and DsRed (optically absorbing, naturally fluorescent protein) on silica surfaces. Specifically, we propose synthesis of thin protein layers by means of dip coating of the dielectric surface in protein solutions with different concentrations (0.01–5.0 g l^{-1}). We employed spectroscopic ellipsometry as the most suitable and non-destructive technique for evaluation of the protein layers' thickness and optical properties (refractive index and extinction coefficient) after dehydration, using two different optical models, Cauchy for BSA and Lorentz for DsRed. We demonstrate that the thickness, the optical properties and the wettability of the thin protein layers can be finely controlled by proper tuning of the protein concentration in the solution. These results are correlated with the thin layer morphology, investigated by AFM, FTIR and PL analyses. It is shown that the proteins do not undergo denaturation after dehydration on the silica surface. The proteins arrange themselves in a lace-like network for BSA and in a rod-like structure for DsRed to form mono- and multi-layers, due to different mechanisms driving the organization stage.

Keywords: SiO_2 thin layers, proteins, protein-adhesion problem, protein thin layers, BSA, DsRed

1. Introduction

In the last ten years, the research and development of new biomaterials based on oxides, such as silicon oxide-related materials, has considerably increased. The growing interest in this field is due to the use of biomaterials in well-established applications in medicine for anti-bacterial coatings of orthopedic and dental implants or for *in vivo* labeling and drug screening systems [1–3]. Newly created niche applications of biomaterials are currently gaining pace. They are mainly related to bioelectronics, to proteins engineering, dealing with generation of function-specific proteins for tissue engineering

and therapeutics, or more generally to nanotechnology where the properties of inorganic and organic solid materials should be adapted to those of proteins [4–7].

Regardless of the targeted application, whenever a foreign material is brought to a contact with blood or physiological fluids one of the first process to occur is protein adsorption on the material surface. The conformation and arrangement of the adsorbed proteins further control the subsequent biological processes and thus determine the biological response to the material [8–11]. Protein adsorption on solid surfaces manifests both beneficial and adverse effects depending on the application, including cell attachment and biofouling, respectively [12–15]. It depends on different factors related to both the protein itself and the surface as the final outcome is shared between the two sides [11, 16]. A large number of variables, like surface energy, wettability, electrical charge, temperature, buffer pH, time, kind of studied protein, etc, is at play and can substantially affect the experimental results, which actually complicates the comparison from study to study. Consequently, the protein adsorption on solid surfaces remains an intensive field of research supported by the interest in revealing the underlying mechanisms and possible applications [11, 17–20]. Many years of research on the 'protein-adsorption problem' however conducted to identification of some common trends which are generally related to the internal coherence of the proteins. Structural rearrangements do not significantly contribute to the adsorption process for 'hard' proteins, i.e. for proteins with strong internal coherence. These proteins behave like 'hard' particles and their interaction with the solid surface is governed by hydrophobic and electrostatic effects [11, 17, 18]. They tend to adsorb to hydrophobic surfaces but their adsorption on hydrophilic surfaces is attained only if they are electrostatically attracted. On the contrary, the so called 'soft' proteins, i.e. proteins of much lower structural stability are apt to adsorb even under unfavorable conditions. The 'soft' proteins are found to adsorb freely also on hydrophilic and electrostatically repulsing surfaces.

The 'protein-adsorption problem' is of fundamental nature and becomes of primary importance when the interactions with silicon oxide-related materials are under study. The SiO_2 is an inorganic material with strongly pronounced hydrophilic properties, thus not favoring protein adsorption. SiO_2 is well known for its optically transparent properties in the visible range of the spectrum and can successfully be used as anti-reflective coating if properly dimensioned. The interest towards SiO_2 layers is also based on their large application in plasmonics as host matrix, in microelectronics as diffusion or thin electrical insulating layers, etc [21–24]. Although many studies have been devoted to exploring the biocompatibility of silicon oxides *in vivo* or *in vitro*, the reported results on the physico–chemical properties that drive or influence their biocompatibility remain limited. A deeper understanding of the physico–chemical properties and the basic principles of the complex material-biological interactions is under request, especially when biosensing and/or CMOS-compatible bioelectronic devices are forecasted as potential applications.

In the present work, we report on the adsorption behavior of two different, in their internal coherence, proteins after adhesion and dehydration on thin silica layers through spectroscopic ellipsometry (SE) coupled with investigation of their optical and structural properties. It comes out with study on bovine serum albumin (BSA) and *Discosoma* recombinant red fluorescent protein (DsRed). The BSA is a 'soft' and small protein that was chosen as a model protein because of its high abundance in the blood plasma, from one side, and because it readily adsorbs on foreign surfaces dominating the first stages of proteins adsorption [25, 26] from the other side. Moreover, the BSA is optically non-absorbing protein. The second selected protein is the recently cloned from reef coral *Discosoma* sp. DsRed protein [27]. The DsRed belongs to the naturally fluorescent protein family. It is found to be suitable for rational design of ultra-stable and reversible photoswitchable devices for super-resolution imaging [28] and holds great promises for biotechnology and cell biology as a spectrally distinct companion or substitute of the green fluorescent protein.

2. Materials and methods

2.1. Thin SiO_2 sample preparation

Silica layers of about 100 nm-thick were thermally grown on intrinsic Si-substrates at 1100 °C under slightly oxidizing atmosphere using a N_2–O_2 gas mixture containing 1.0% of O_2. Before being exposed to protein deposition, the SiO_2/Si substrates were consecutively cleaned in ethanol (95% vol.) and acetone (95% vol.) and then rinsed in deionized water to avoid electrostatic interactions and to permit a better control of the experimental conditions. The deionized water was filtered through 200 nm pore size filter. The rinsing procedure continued until attaining zero surface conductivity on the SiO_2 surfaces.

2.2. Selected proteins and preparation procedure

BSA has been chosen as a model protein to start the synthesis of very thin protein layers on solid substrates. BSA was purchased from Sigma Aldrich. According to the SDS-PAGE, the BSA was at least 96% pure in a lyophilized powder form. A stock solution of BSA was prepared with a concentration of 5.0 g l^{-1} in 50 ml water for injectable preparations (PPI water, European Pharmacopoeia, COOPER) [29]. The pH-value of the PPI water was measured to 7.0 with conductivity of 1.2 μS cm^{-1}. The pH-value of the BSA stock solution was measured to 5.6, whilst the BSA isoelectric point (pI) is reported to be 4.7 in water and at 25 °C. Aliquots of BSA stock solution were then diluted 1–500 times in PPI water.

The second selected protein for this work was the naturally fluorescent DsRed. DsRed was purchased from Biovision and according to the SDS-PAGE, it was at least 97% pure and in a freeze-dried form. DsRed stock solution of 0.1 g l^{-1} was prepared in PPI water. Aliquots of DsRed stock solution were diluted 1–10 times into PPI water. The pH-

value of the DsRed stock solution was measured to 6.6 and its stability was continuously monitored during the measurements. The assays were performed at room temperature (23 °C).

While BSA has a size of 4 nm × 4 nm × 14 nm (prolate spheroid shape where $a = b < c$) [1, 26], DsRed, that is generally under tetrameric form in solution and in the crystal, is a squat rectangular prism comprising four monomers consisting of an 11-stranded β-barrel with a coaxial α-helix where the chromophores are arranged in c.a. 2.7 nm × 3.4 nm rectangular array in two approximately antiparallel pairs [30].

2.3. Deposition of thin protein layers

Thin protein layers on silica surfaces were prepared by dip coating process. Basically, SiO_2 thin substrates (80–105 nm) with a fixed superficial area of 1 × 1 cm^2 were immersed for 1 h in 1 ml of the protein solutions; seven different concentrations were prepared for the BSA solution (0.01 g l^{-1}, 0.05 g l^{-1}, 0.1 g l^{-1}, 0.5 g l^{-1}, 1.0 g l^{-1}, 2.5 g l^{-1}, 5.0 g l^{-1}) and three for DsRed (0.01 g l^{-1}, 0.05 g l^{-1}, 0.1 g l^{-1}). After the immersion, the samples were rinsed in PPI water to remove all the non-adhered proteins and were left dehydrating at room temperature and atmospheric pressure before starting the physico–chemical characterization.

2.4. Wettability measurements of thin protein layers

Sessile droplets of PPI water of a very small volume (2.5 ± 0.1 μl) were brought to contact with the surface of the thin dehydrated protein layers deposited on the SiO_2 substrates to investigate their wettability. The contact angle was measured using Digidrop goniometer from GBX Scientific Instruments. The droplets were deposited with microsyringe Gastight 1700 series fixed on the goniometer giving the possibility of fine control of the droplet volume. To record and analyze the droplets a Visiodrop software was coupled to the contact angle meter. The measurement precision of the applied method is of ±0.1°. The results given in this work are averaged over three independent measurements per sample.

2.5. Structural and optical characterizations

Absorption spectra of the protein solutions were obtained from optical transmittance measured at room temperature by a Hewlett Packard HP8452A Diode Array UV–vis spectrophotometer in the range 190–820 nm to evidence the differences between the optical properties of the two investigated proteins and, in the meantime, to validate the choice of the best optical model required for the ellipsometric simulations.

Optical images of protein thin layers after their dehydration were recorded with a digital microscope Keyence VHX-1000 using the VHX 1.3.0.7 associated software to get information on their morphological state at the micrometric scale.

Topography images were acquired with a Bruker Multimode 8 set-up using Peak-Force Quantitative NanoMechanical (PF-QNM) mode. To probe soft material as the resulting protein layers a SNL tip with spring constant of 0.24 N m^{-1} and curvature radius of around 5 nm was used. The peak force was set to 0.5 nN.

Fourier transform infrared (FTIR) spectra were acquired with a Brucker Vertex 70 spectrometer in transmission mode in the range 400–4000 cm^{-1} with a resolution of 2 cm^{-1} to obtain information about the composition of the dehydrated protein layers. The transmission mode was attainable owing to the transparency to infrared light of the used intrinsic Si-substrates.

The photoluminescence (PL) spectra were acquired under 532 nm excitation wavelengths with a confocal Jobin-Yvon XploRa equipment. In order to avoid possible degradation of the molecules due to laser heating, the incident intensity was limited to 10% (1.5 mW) of its maximum value. The laser beam was focused down to 2 μm spot diameter using a 50× objective, by which also the emitted light was collected. Then, it was dispersed using a Jobin Yvon spectrometer with a 600 grooves mm^{-1} grating. A mapping of the PL intensity was performed using a piezoelectric stage at the same experimental conditions in an area of 40 × 40 μm^2, with a scan step of 5 μm.

For the SE measurements, a Semilab ellipsometer SE-2000 with a rotating polarizer and a fixed analyzer was used in the spectral range 250–850 nm. To maximize the accuracy in the recorded spectra during SE measurements, the incident angle was set to 75° which appears to be the most appropriate for Si substrates. It gives the largest phase shift Δ between the parallel and the perpendicular components of the polarized electric field after reflection. All measurements were carried out between 250–850 nm in steps of 5 nm. After the data acquisition, numerical analysis was required to extract the information concerning the protein layer. However, for any such procedure to succeed, it is necessary that accurate data for the 'known' parameters are available. The most important of these parameters is the dielectric response ε of the substrate. For this reason, we characterized the substrate properties (especially thickness of the thin SiO_2 layer) through SE measurements before the protein layers were deposited. Then, the simulation of the recorded spectra was performed with SE Analyzer-SEA (WinElli 3) software [31] provided by Semilab. A three-phase model was used to characterize the dielectric SiO_2 on Si substrates. However, for the protein layers, a proper choice of the simulation model for the dispersion law, depending on the protein optical properties, was made and it will be discussed along the paper. In the following section, a focus on the two main used models is reported.

3. SE for proteins adsorption study. Short overview of theory and models

In the present study, SE was extensively used to analyze the optical properties of the protein layers deposited on SiO_2. SE is an optical technique based on the measurements of the polarization changes occurring upon reflection at oblique incidence of a polarized monochromatic plane wave. It is

largely applied to study the optical response of thin layers. SE is a non-destructive, low-cost diagnostic method and quite appropriate to follow (*in situ*) and to control (*in situ* and/or *ex situ*) the thicknesses and the optical properties of thin transparent layers. The basic quantity measured with SE is the complex reflectance ratio $\rho = \chi_r/\chi_i$ where χ_r and χ_i represent the state of polarization of the reflected and incident beam, respectively. For optically isotropic samples this equation simplifies to $\rho = R_p/R_s = \tan\Psi\ e^{i\Delta}$ where R_p and R_s are the complex reflection coefficients for light polarized parallel and perpendicular to the plane of incidence, respectively. The directly measured parameters are $\tan\Psi$ and $\cos\Delta$, where Ψ and Δ are called ellipsometric angles. In particular, $\tan\Psi$ represents the ratio between moduli of the reflection coefficients, meaning that it is closely related to the changes in the amplitudes of the polarized electric field after reflection and $\cos\Delta$ gives the phase difference ($\Delta = \delta_p$–δ_s) between the perpendicular (δ_s) and parallel (δ_p) components of the polarized electric field, induced by the reflection. It is also worthy to point out that the SE is an indirect technique, meaning that to extract the desired information from the experimental data, such as materials complex dielectric functions $\varepsilon = \varepsilon_1 + i\varepsilon_2$ (or refractive index $n = \sqrt{\varepsilon}$, both functions of the photon energy) and thickness, an appropriate optical model should be taken into account [32]. SE was intensively applied to study the adsorption of proteins on solid surfaces [33–40]. It appears also as a very suitable characterization technique for sensor applications where physico–chemical effects as biointeraction, internal adsorption, *etc* are under study in immunosensors, DNA-hybridization [35]. To model the protein layers on the dielectric substrates, we recurred to the so-called four-phase model, the specific configuration consisting of the following phases: (1) Si substrate; (2) the silica thin layer (80–150 nm); (3) the thin protein layer; and (4) the surrounding medium (air). Once the proper optical models for describing the layers were chosen, the ellipsometry data were fitted to the model with the Levenberg–Marquardt algorithm to minimize the root mean squared error that measures the regression quality and, consequently, the goodness of the fit. The surface mass concentration of the protein layers, Γ, was then calculated according to the de Feijter's formula [36], using the calculated refractive index of the protein layers at 632.8 nm.

3.1. Cauchy model

For all proteins that do not display optical absorption in the visible spectral range, the most suitable dispersion law for ellipsometric spectra simulation is the transparent Cauchy model. The refractive index is characterized by a real part (n) that decreases monotonously by increasing the wavelength, and the imaginary part being null, $k = 0$, by following the relation:

$$n(\lambda) = A + \frac{B}{\lambda^2} + \frac{C}{\lambda^4}, \tag{1}$$

where A is a dimensionless parameter describing the material refractive index for $\lambda \to \infty$, while B (in nm^2) and C (in nm^4) affect the amplitude and the curvature of the refractive index in the visible and UV wavelength ranges, respectively. Generally, $A > 1$ and $0 < C < B < 1$ [1]. This model has been mostly employed to study the structure of non-absorbing layer of biotin–avidin [37] and ferritin [38] and it is also the most suitable for albumin [39], such as BSA, since this protein does not display any optical absorption in the visible range [1, 40, 41].

3.2. Lorentz model

For weakly absorbing proteins in the visible spectral range, Cauchy law cannot be employed. For this reason, we recurred to the Lorentz dispersion law. It is generally used for describing frequency dependent polarization due to bound charge. It is suitable for absorbing proteins because it well describes radiation absorption due to interband transitions where electrons move from a ground state to a final state without changing their **k**-wavevector in the Brillouin's first zone. To simulate the complex dielectric function $\tilde{\varepsilon}(\omega)$ of a material, the Lorentz model considers the response of a dipole to a submitted electromagnetic field assuming that the electrons oscillate according to a damped harmonic oscillator. By resolving the equation for the electrons motion, it is possible to extract the expression of the oscillation amplitude $\vec{r}$ and hence the complex dielectric response as a function of the photon pulsation ω. This is directly connected with the material's susceptibility $\chi(\omega)$ through the relation:

$$\chi(\omega) = \frac{-e\,N\,\vec{r}(\omega)}{\varepsilon_0\,E(\omega)}, \tag{2}$$

where N is the total number of dipoles per unit volume in the material, $E(\omega)$ is the incident electromagnetic field, e is the electron charge, and ε_0 is the vacuum permittivity. The complex dielectric function can be extracted thus by knowing $\vec{r}(\omega)$:

$$\begin{aligned}\tilde{\varepsilon}(\omega) &= 1 + \chi(\omega) = 1 + \frac{-e\,N\,\vec{r}(\omega)}{\varepsilon_0\,E(\omega)} \\ &= 1 + \frac{\omega_p^2}{\omega_t^2 - \omega^2 + i\gamma_0\omega},\end{aligned} \tag{3}$$

where γ_0 is defined as the damping factor in the oscillation, ω_t is the oscillator resonance frequency, $\omega_p = \sqrt{\frac{N\,e^2}{\varepsilon_0\,m}}$ is the plasma frequency and m the electron mass. This model was employed to estimate the thickness and the optical parameters of optically absorbing proteins, such as in the case of the modification of BSA by absorbing Coomassie brilliant blue dye [42] and of the investigation of the adhesion of blood plasma proteins on hydrogenated carbon thin films [43].

4. Results

4.1. Morphology of the dehydrated thin protein layers

To obtain information on the organization and uniformity of the protein layers, the samples containing a protein layer

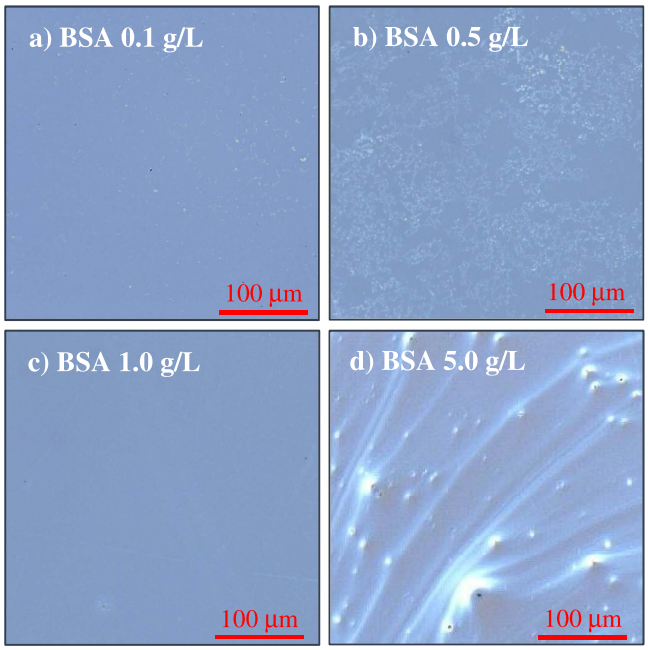


Figure 1. Optical micrographs (pseudocolor images) of bovine serum albumin (BSA) thin layers with different solution concentrations: (a) 0.1 g l^{-1}, (b) 0.5 g l^{-1}, (c) 1.0 g l^{-1} and (d) 5.0 g l^{-1} after adsorption and dehydration at room temperature and atmospheric pressure on top of 100 nm thick SiO_2 substrates. All micrographs were acquired using 500× magnification.

adsorbed and dehydrated on silica thin layers were analyzed by means of optical microscopy under 500× magnification. Although it is difficult to evidence alteration of the proteins structure, due to the limited spatial resolution of the technique and to the nanometric size of the proteins, the characteristic patterns of the protein layer formation at micrometric scale can be deduced.

The optical micrographs corresponding to different BSA concentrations (0.1, 0.5, 1.0 and 5.0 g l^{-1}) are reported in figures 1(a)–(d). As far as the morphology of BSA thin layers is concerned, starting from 0.1 g l^{-1} concentration, one can observe the presence of branched objects with white contrast (figures 1(a) and (b)), that completely disappear at 1.0 g l^{-1} (figure 1(c)). Those patterns are most likely due to discontinuity in the protein layer or to small protein agglomerates. Further increase of the protein concentration ($\geqslant$2.5 g l^{-1}) leads to a non-uniform layer, characterized by peaks and dips, due to the formation of big protein agglomerates on the silica surface (figure 1(d)).

At the microscopic scale a comparison between the BSA and DsRed thin layers, resulting from the same concentration of 0.05 g l^{-1}, is presented in figures 2(a) and (d). For the DsRed layer at low concentration one observes a partial coverage of the surface, as already evidenced for the BSA layers, with the proteins being concentrated close to the whitish spots. Only protein aggregates were visible by optical microscopy. Statistical analysis performed on more than 300 agglomerates reveals that the average distance between the aggregates is 18.5 μm with a spread of 11.2 μm for the DsRed thin layer with a concentration of 0.05 g l^{-1}.

To achieve information at the nanoscale on the organization stage of the two protein layers an AFM investigation was performed in PF-QNM mode (figures 2(b) and (e)). Comparison of the resulting BSA and DsRed protein layers shows different behavior in the adsorption process. Indeed, the BSA proteins arrange themselves in a lace-like network whereas the DsRed proteins exhibit a rod-like structure. These organizations were further probed on smaller regions presented in figures 2(c) and (f). For the BSA protein, the height histogram (insert of figure 2(c)) shows a value of 4.3 nm between the substrate surface and the protein layer. This value is consistent with the BSA smaller dimension (minor axis of the spheroid) [1, 26] suggesting that the proteins are 'side-on' adsorbed on the surface. For this concentration of the BSA solution (0.05 g l^{-1}) the resulting BSA layer is mainly constituted by a mono-layer structure. Concerning DsRed, the height histogram presented in the insert of figure 2(f) shows a value of 3.6 nm between the substrate and the protein layer. The obtained value is consistent with the protein monomer dimension [30]. Moreover, a much less intensive second peak is observed at 7.2 nm (twice the 3.6 nm) which corresponds to a layer formed by proteins in their tetrameric form. Accordingly, the DsRed layer resulting from the same concentration in the solution (0.05 g l^{-1}) is constituted mainly by monolayer of monomers with small residues of tetramers.

4.2. Light interactions with thin protein layers

Investigation of the optical properties of the dehydrated protein thin layers after interaction with light can give further information on the protein adhesion mechanisms. Firstly, we investigated the optical absorbance of the protein solutions used for the growth of the protein thin layers. The spectra reported in figure 3 show the main absorption peaks of the DsRed fluorescent protein and the BSA model protein. In the BSA absorption spectrum only some weak optical structures due to π–π^* transitions in the aromatic amino acid residues near 280 nm and the general peptide backbone UV absorption below 250 nm can be observed [26], while otherwise the optical response of BSA is rather featureless in the visible range. Differently, DsRed absorption spectrum presents a broad band extended between 445–575 nm (convoluted in two peaks), overlapped with the UV ones at 280 nm and below 250 nm. It should be pointed out that the red fluorescence of DsRed takes several days to mature, passing through an obligatory green fluorescent intermediate [44]. Furthermore, the DsRed tetramer, during its maturation, consists of oligomers of both an immature, green emitting form, and a mature, red-emitting form. Therefore, the broad DsRed absorption band in the visible range can be interpreted as convolution of the absorption bands of immature green and mature red chromophores, respectively peaked at 480 and 558 nm with an overall full width at half maximum (FWHM) of about 135 nm. The large difference between the BSA and DsRed absorption spectra in the visible

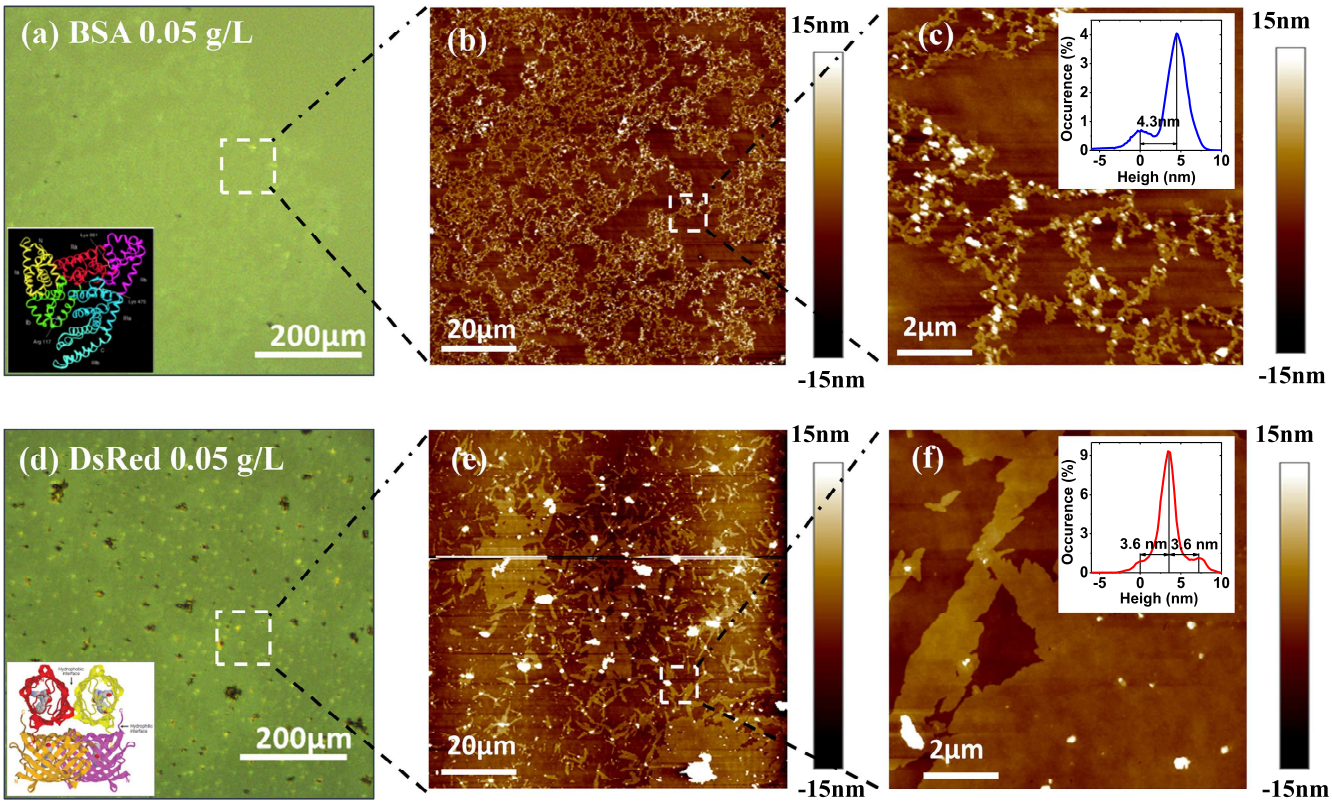


Figure 2. Top line: BSA protein thin layer after adsorption and dehydration at room temperature and atmospheric pressure on top of 100 nm thick SiO_2 substrates (solution concentration of 0.05 g l^{-1}), in (a) optical micrograph in pseudocolors, in insert an image of BSA; AFM scan (height amplitude) over (b) 100 μm × 100 μm region, (c) 10 μm × 10 μm region (in insert height histogram); bottom line: DsRed protein thin layer (0.05 g l^{-1}), in (d) optical micrograph in pseudocolors, in insert an image of DsRed; AFM scan over (e) 100 μm × 100 μm region, (f) 10 μm × 10 μm region (in insert height histogram).

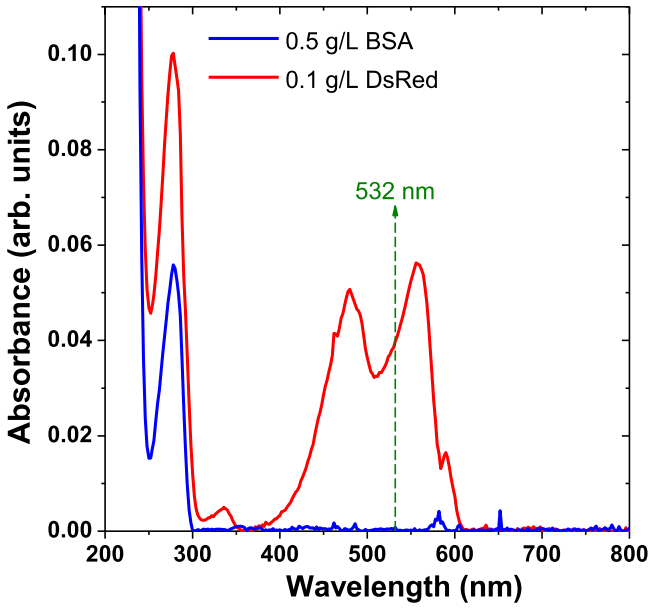


Figure 3. Absorption spectra of BSA (0.5 g l^{-1}) and DsRed (0.1 g l^{-1}) solutions. The absorption peak at 280 nm, present in both solutions, is due to the π–π^* transitions in the aromatic amino acid residues. While the BSA is transparent in the visible range, the DsRed has two convolved absorption peaks related to the chromophores.

range will be considered for the simulation of the ellipsometric spectra, with the aim to extract the layer thickness and the optical parameters. Unfortunately, the absorption spectra of dehydrated protein layers were not accessible due to the very thin protein layer formed by means of dip coating. This would have also given further information on the secondary structure of the proteins. To overcome this issue, we have performed FTIR and PL measurements (where applicable) on the dehydrated layers.

The recorded FTIR spectrum of the dehydrated protein layers [45] is reported in figure 4(a) only for the highest concentration 5.0 g l^{-1} of BSA. For smaller concentrations, there is no enough matter to detect any signal rather than silica, owing to the small BSA layer thicknesses. In the same way, the only accessible information was gathered on DsRed dehydrated layer with concentration of 1.0 g l^{-1}. In the same figure, we have also reported as reference the FTIR spectrum of the thermal silica layer used as a substrate. The typical bond vibrations of the SiO_2, such as the Si–O–Si rocking vibration at 457 cm^{-1}, the symmetric stretching mode at 810 cm^{-1} and the asymmetric stretching mode at 1067 cm^{-1} [46] are easily recognizable. In addition to the SiO_2 signature, in the FTIR spectrum of BSA protein thin layer it is also possible to identify other features, although overlapped with the most intense silica FTIR signatures: the band between

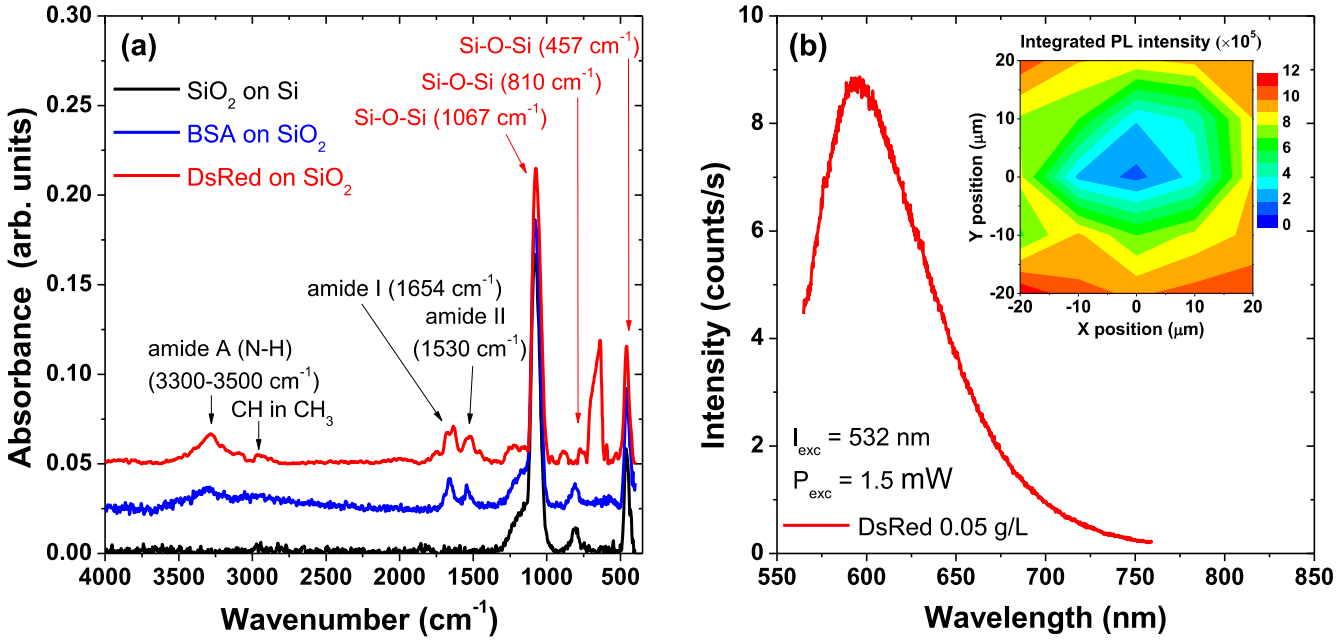


Figure 4. (a) FTIR spectra of dehydrated BSA (5.0 g l^{-1} solution) and DsRed (1.0 g l^{-1} solution) thin layers on SiO_2 substrate. In addition the FTIR spectrum of the SiO_2 is reported; (b) photoluminescence spectrum from DsRed (0.05 g l^{-1} solution) dehydrated thin layer under 532 nm excitation. In the inset, a mapping of the PL intensity over a region of 40 × 40 μm^2 is reported.

1600–1700 cm^{-1} is ascribed to the C=O stretch vibrations of the peptide linkages and it is highly sensitive to the protein secondary structural components. Occurrence of proteins denaturation and unfolding processes after dehydration leads to a complete loss of the proteins secondary structure and, therefore, the disappearance of these typical FTIR signatures. However, from the FTIR spectrum acquired on the dehydrated layers of BSA and DsRed, the Amide I band with peaks centered at 1654 cm^{-1} and the Amide II band centered at 1530 cm^{-1} assigned the protein α-helix are still well distinguishable [45, 47], thus permitting us to deduce that the protein secondary structure is preserved after adsorption, adhesion and dehydration on the silica substrate. The other broad bands at about 3300–3500 cm^{-1} and 2800–3100 cm^{-1} on the spectra can be instead related to the Amide A (N–H) and the C–H bonds in CH_3 environment, respectively.

Taking advantage of the fact that DsRed belongs to the family of naturally fluorescent proteins, we could exploit photoemission spectroscopy to investigate whether the proteins were or not denaturated. Indeed, in absence of denaturation and unfolding of the proteins, the DsRed are supposed to emit in the orange–red wavelength range [27]. To obtain this information, the excitation wavelength of 532 nm was used to excite selectively only the DsRed mature red species without contributions from the immature green chromophores. The PL spectrum obtained for the DsRed dehydrated thin protein layer with the protein concentration of 0.05 g l^{-1} is reported in figure 4(b), where the presence of an intense red emission peaked at 594 nm can be observed. The PL emission from dehydrated DsRed layers scales up linearly with the protein concentration up to 0.25 g l^{-1}. For higher protein concentrations quenching is observed [45]. Although the peak of PL emission is slightly shifted compared with the values reported in the literature for luminescence coming from solutions (583 nm) [27], likely due to the dehydration process, we could straightforwardly conclude that for DsRed proteins the secondary structure is preserved after adsorption, adhesion and dehydration on silica substrates. Thus, the PL spectroscopy for fluorescent proteins can be claimed as a non-destructive and strongly sensitive method to detect the status of a protein, being complementary to the FTIR study. The inset of figure 4(b) reports a PL map over a 40 × 40 μm^2 area. The intensity variation that can be observed (around one order of magnitude among the central region and the edges in the map) reflects the non-uniform distribution of DsRed proteins on the surface (for concentration of 0.05 g l^{-1}). The mean distance among the most luminescent points on the map has been found to be around 20 μm, which is compatible with the mean distance between DsRed agglomerates observed in the optical micrograph (figure 2(d)).

4.3. SE on thin protein layers

The SiO_2 surface is hydrophilic to PPI water [45], indicating that the protein molecules bind with fewer conformational changes and consequently give rise to a less space-filling [11, 17, 18]. Moreover, it is believed that the presence of protein layers has strong consequences on the biofilm formation and growth on surfaces in the biomedical domain. For the above reasons, the control of the protein layer thickness is a very important step aiming at a thorough understanding of the underlying mechanisms of the adhesion phase. To track the protein adhesion process and measure the thickness of the resulting protein layer we used a non-destructive and non-invasive optical technique, namely the SE. The obtained results can be moreover correlated with the ones obtained by

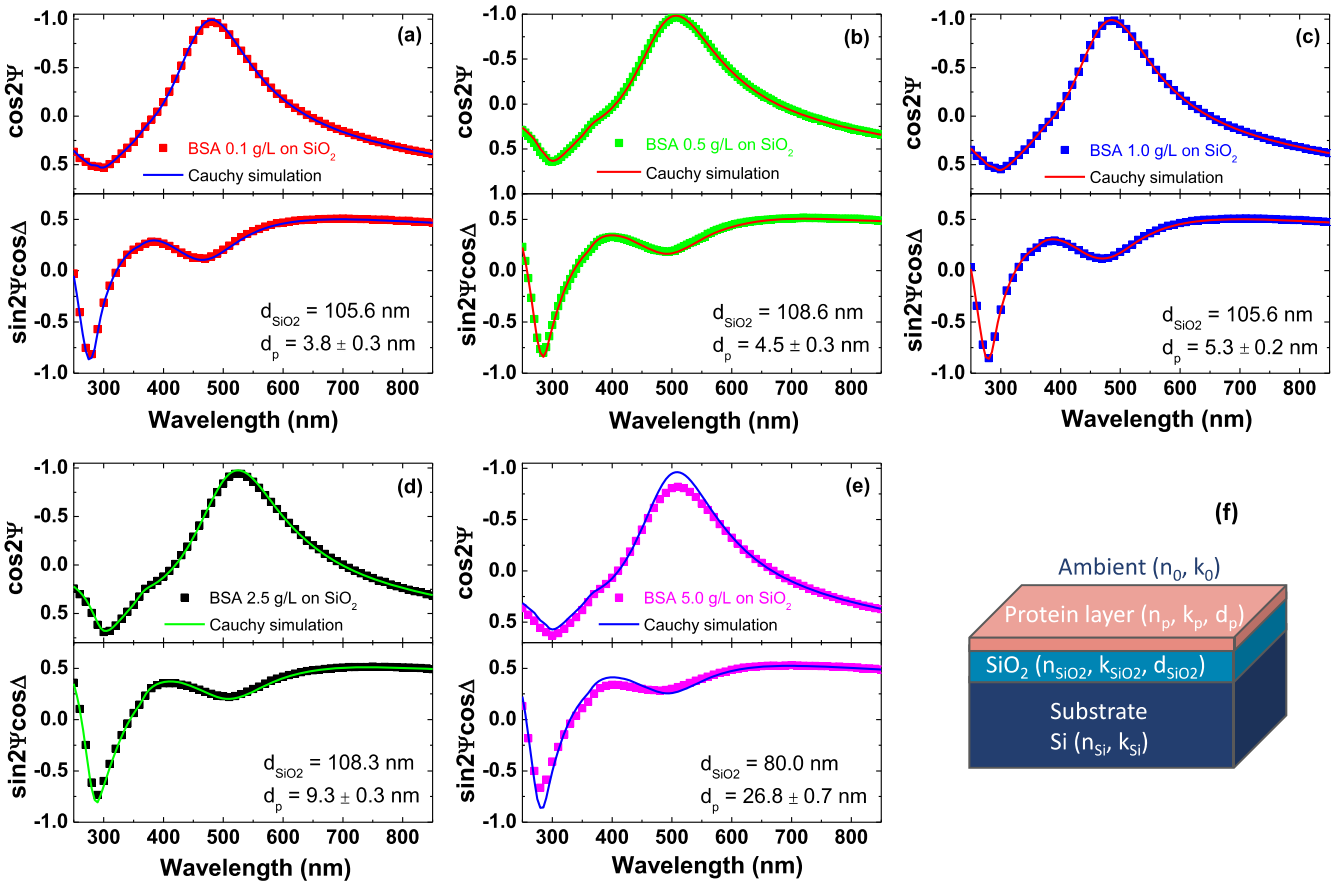


Figure 5. (a)–(e) Ellipsometric spectra of BSA thin layers formed after dehydration for different solution concentrations (0.01, 0.5, 1.0, 2.5 and 5.0 g l^{-1}), (f) schematic representation of the modeled structure.

means of AFM PF-QNM measurements and from the investigation of the optical and structural properties shown in the previous sections. As explained in section 3, an important point in this study was to evaluate the relevance of different theoretical models necessary for the interpretation of the recorded ellipsometric spectra in terms of optical absorbance of the studied protein.

The ellipsometric spectra measured after BSA adsorption on thin silicon oxide layers are reported in figures 5(a)–(e). Before the thin protein layer deposition, the thickness of the thermal silicon oxide used as substrate was precisely measured to improve the accuracy in the measurement of the protein layer thickness. The observed slight difference between the ellipsometric spectra before and after the growth of protein layer actually contains the information about the amount/thickness of the adsorbed BSA proteins forming the protein layer for different BSA concentrations. For the sake of simplicity only the spectra corresponding to the total structures are presented in the graphs. Schematic representation of the modeled structure is presented in figure 5(f). The measured thickness of the SiO_2 layer was thus fixed in the modeling of the total structure. Since the BSA is an optically non-absorbing protein in the visible wavelength range (figure 3), the spectra were simulated using the Cauchy law.

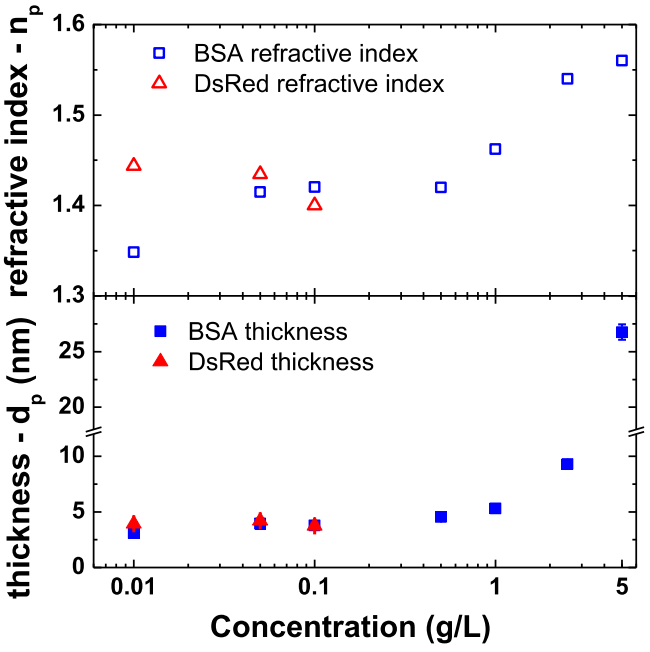


Figure 6. Refractive index (upper part) and thickness (lower part) of the adsorbed protein layers on SiO_2 after 1 h immersion for different BSA and DsRed concentrations.

Table 1. Data extracted from ellipsometry measurements of BSA and DsRed thin layers.

Conc. (g l^{-1})	Refractive index (n) @632 nm	Thickness d_p (nm)	R^2	RMSE	Γ (μg cm^{-2})
BSA					
0.01	1.35	3.1 ± 0.2	0.999 45	0.007 92	0.047
0.05	1.42	3.9 ± 0.1	0.999 42	0.008 22	0.199
0.1	1.42	3.8 ± 0.3	0.999 37	0.008 50	0.203
0.5	1.42	4.5 ± 0.3	0.9994	0.008 47	0.243
1.0	1.46	5.3 ± 0.2	0.999 52	0.007 32	0.455
2.5	1.54	9.3 ± 0.3	0.997 17	0.018 48	1.004
5.0	1.56	26.8 ± 0.7	0.977 27	0.052 02	3.434
DsRed					
0.01	1.44	3.9 ± 0.1	0.999 67	0.007 39	0.259
0.05	1.44	4.2 ± 0.1	0.999 49	0.007 53	0.257
0.1	1.40	3.7 ± 0.2	0.999 58	0.007 14	0.160

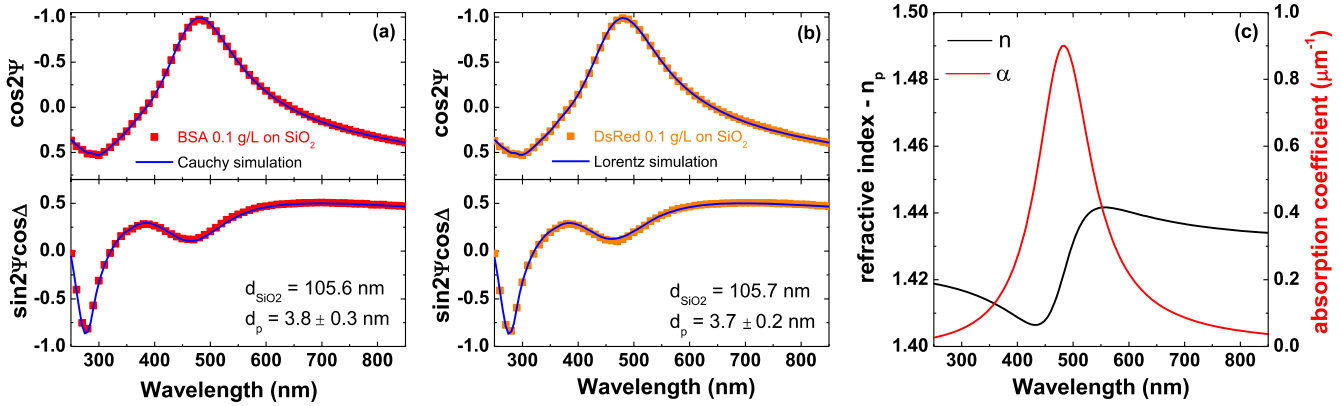


Figure 7. Comparison between the optical spectra of BSA (a) (Cauchy law, non-absorbing proteins) and DsRed (b) (Lorentz law, absorbing proteins) at the same protein concentration (0.1 g l^{-1}). (c) The DsRed complex refractive index (n) and absorption coefficient (α) extracted from the simulation is reported.

The protein layer thickness and its refractive index for different protein concentrations in solution, extracted during the simulation process, are reported in figure 6 as well as summarized in table 1. It is possible to observe that the thickness slightly increases by increasing the BSA concentration from 0.01 to 0.05 g l^{-1} and remains almost unchanged when increasing the protein concentration up to 0.1 g l^{-1}. After 0.1 g l^{-1}, the thickness increase is more evident and it becomes steeper above 2.5 g l^{-1}. Also the protein refractive index increases slightly by increasing the solution concentration. Thus, considering the refractive index n_p obtained for protein layers as an indication of the BSA layer density, we can claim that the densest layers are formed above 2.5 g l^{-1}, while for the lowest concentration of 0.01 g l^{-1} the formed layer is likely porous. This last result, coupled with the absence of evident changes in the BSA protein layer thickness in the range 0.01–0.1 g l^{-1}, suggests that for these concentrations the protein layer starts to form itself by filling the voids and becoming denser. It is also consistent with the AFM PF-QNM topography measurements showing that for low BSA concentrations in the solution the resulting protein layer organizes in a lace-like network.

The ellipsometric spectrum of the adsorbed layer of DsRed at 0.1 g l^{-1} in solution is reported in figure 7, in comparison with the BSA one at the same protein concentration as an example. The similar spectra shape suggests that the two layers have comparable thicknesses. However, since the DsRed is an optically absorbing protein in the visible wavelength range, the Lorentz model was found to be more appropriate than the Cauchy model for simulating its response after light irradiation.

The Lorentz simulation gave a value of 3.7 ± 0.2 nm for the DsRed thin protein layer thickness, compatible with the DsRed monomer size. A scan of the thickness in an area of several mm^2 was also performed to probe its uniformity. The scan resolution was of 100 μm determined by the size of the light spot. In addition, the DsRed thin protein layer complex refractive index was extracted during the simulation process, and it is reported in figure 7(c). In particular, its complex part, the extinction coefficient-k, that reflects the absorption coefficient-α of the investigated materials, is characterized by a main peak at 490 nm and a FWHM of 130 nm, compatible with the FWHM of the DsRed absorption band in solution reported in figure 3. It is worth pointing out that it was not possible to simulate the experimental spectra with a double-

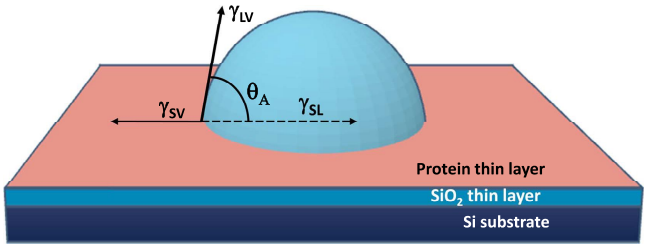


Figure 8. Schematic representation of the wettability tests performed on thin protein layers where γ_{SL} is the solid–liquid interface, γ_{SV} is the solid–vapor interface and γ_{LV} is the liquid–vapor interface, θ_A is the advancing angle.

peak Lorentz model, such as the absorption spectrum from solution would suggest. Our understanding on the issue is that during the adhesion and dehydration processes the optical properties of the DsRed thin layers change slightly compared with the ones of the proteins in solution. Therefore the two absorption peaks become closer and larger during the dehydration, resulting in a convoluted absorption band. This hypothesis is supported also by the shift of about 10 nm in the PL emission peak (594 nm) shown in figure 4(b), compared with the values found in literature for PL of DsRed from solution (583 nm) [27].

The protein layer thicknesses alongside with the corresponding refractive indexes and surface concentrations extracted during the simulation process are reported in figure 6 as well as in table 1 for the other investigated concentrations of DsRed: 0.01 and 0.05 g l^{-1}. Similarly to the BSA thin layers, by using SE we did not observe any significant variations in the resulting thin layer parameters (thickness, refractive index, surface concentration) with increasing the DsRed protein concentration in the range 0.01–0.1 g l^{-1} (figure 6).

4.4. Wettability of dehydrated thin protein layers

In biomedical applications, microbial adhesion and biofilm formation represent a major complication in implanted and percutaneous medical devices, and together, they form an important stage in the development of infection with potential septic complications or lethal issues [48]. Moreover, it is well known that protein layers represent the conditioning step for micro-organism adhesion, formation of biofilm and colonization of biomedical surfaces. Therefore, a study on the wettability properties of thin proteins layers is well justified aiming at an identification and description of the underlying mechanisms. With the intention to initiate such study, here we compare the measured advancing contact angles when sessile droplets of PPI water are brought in contact with previously deposited proteins layers, as schematically represented on figure 8. The PPI water, used in this work to dilute the proteins in order to prepare the stock solution for the dip coating process, is indeed used to prepare injectable solutions in human bodies. The idea behind is to investigate the response of dehydrated protein layers to liquids which can be further applied for example for biosensors or in bioelectronic devices.

Figure 9(a) shows the evolution of the measured water contact angles during the dehydration process of the droplets for the obtained thin protein layers of BSA (0.05 g l^{-1}) and of DsRed (0.05 g l^{-1}), compared with the bare SiO_2 surface (control). The advancing contact angle values at $t = 1$ s after the PPI droplet deposition are reported in table 2 together with optical images of the water droplet. While the nature of the SiO_2 surface is hydrophilic ($\theta_A = 63.2°$), the resulting protein layers for this concentration behave as more hydrophobic surfaces, with measured advancing contact angles being $\theta_A = 75.1°$ for DsRed and $\theta_A = 79.9°$ for BSA, respectively thus suggesting a lower wettability of the protein layers than the SiO_2 surface.

It is also worth to notice that while the contact angle of PPI on bare SiO_2 is nearly preserved for the whole dehydration process due to the contact angle hysteresis phenomenon (except for the very end), the contact angles of PPI water on the protein layers decrease linearly with time for both BSA and DsRed [45]. The reported 0°-values on figure 9(a) are for indication purposes only. They correspond to the time of entire dehydration of the deposited PPI water droplet, i.e. the droplet in no more visible (measurable). The PPI droplet dehydration is well pronounced when the droplet is brought to contact with the protein layer. The time is twice shorter compared to the PPI droplet dehydration on bare SiO_2 surface. To go more deeply in understanding the existence of a possible correlation between the thickness of the protein layer and its wettability, we have systematically investigated the behavior of the PPI water contact angles for the different BSA concentrations and reported the trend as a function of the measured proteins thickness, as shown in figure 9(b). As it is possible to observe, when increasing the BSA concentration and, consequently, the protein layer thickness (see section 4.3), the advancing contact angle increases. For BSA concentration included in the range 0.01–0.1 g l^{-1}, the contact angle has almost a linear dependence on the layer thickness and it varies in between 70°–80°, reaching values of 88.13° and 97.47° for 0.5 g l^{-1} and 1.0 g l^{-1}, respectively. The later concentration value can be considered as a saturation point, since for all the other higher concentrations the contact angle varies only slightly (98.19° for 2.5 g l^{-1}), reaching a plateau region. This means that further increasing the protein concentration, i.e. the protein layer thickness, will only result in an increase of the layer thickness without changing the hydrophobicity of the layer. Considering that the immersion time of the silica substrates in the proteins solutions has been kept constant (1 h) for all BSA concentrations, one can conclude that up to 1.0 g l^{-1} the contact angle is strongly influenced by the solutions concentrations that determine differences not only in the layer thickness but also in its conformation. For higher concentrations, even though the proteins layer thickness continues to increase, no influence on the contact angle can be detected, meaning that no further conformational changes on the layer morphology occurred. This preliminary study opens many perspectives on biomedical applications and will be further directed to the

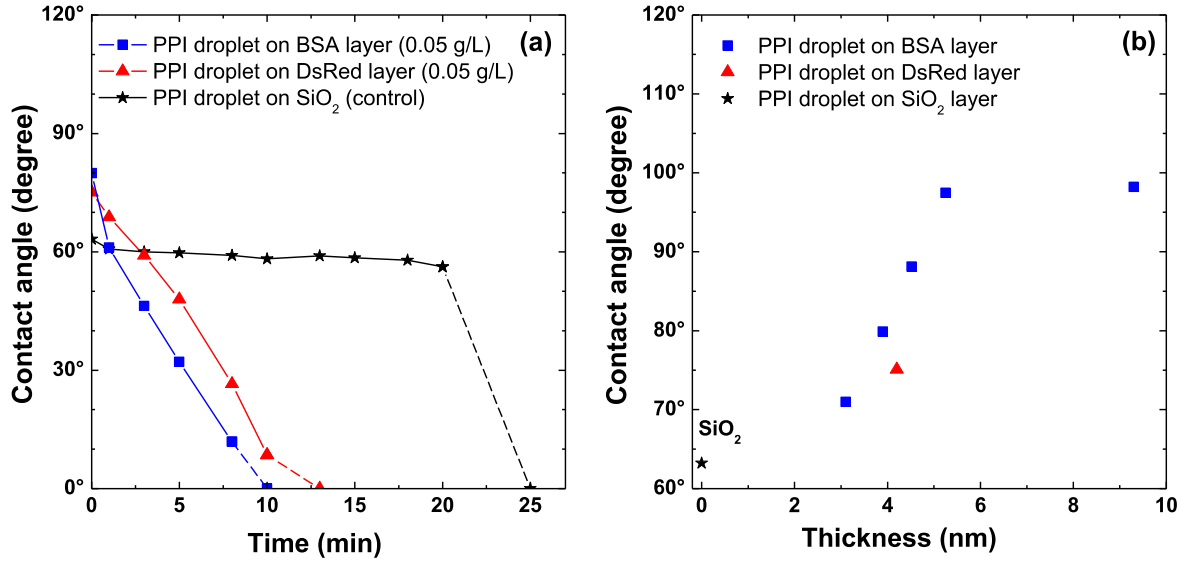


Figure 9. (a) Measured contact angles at 23 °C as a function of time during PPI water sessile droplet dehydration on DsRed and BSA thin layers at the same protein concentration (0.05 g l^{-1}). The behavior of the PPI sessile droplet on a naked SiO_2 substrate is reported for comparison; (b) measured advancing contact angles at $t = 1$ s as a function of the BSA protein layer thickness. DsRed contact angle as a function of thickness is also reported for the concentration of 0.05 g l^{-1}.

Table 2. Advancing contact angles of PPI water droplets when brought to contact with BSA and DsRed layers (0.05 g l^{-1} in solution) and bare SiO_2 layer. The images at $t = 1$ s are also reported.

PPI droplet	SiO_2 surface	DsRed layer (0.05 g l^{-1})	BSA layer (0.05 g l^{-1})
Advancing contact angle (θ_A)	63.2°	75.1°	79.9°
Sessile droplet at $t = 1$ s			

investigation of the micro-organism adhesion in presence of protein thin layers.

5. Discussions

Nowadays, the growing interest in the development of biocompatible materials and on the investigation of the interaction mechanisms of proteins and cells with solid surfaces is highly motivated by their possible applications, in particular for coatings of orthopedic and dental implants, as well as biosensors and bioelectronics. Protein adsorption on oxide materials have been used to evaluate protein adsorption-desorption kinetics in reply to the required assessment of biocompatibility issues [1–3, 49]. Titanium and titanium oxides are the most commonly used materials for the above mentioned applications, due to their appropriate mechanical and chemical properties. The selective adsorption of plasma proteins on hydrothermally grown nano-TiO_2 has already been reported [49], by analyzing the different factors in terms of protein adsorption, such as surface topography and chemical composition, hydrophilic/hydrophobic characteristics, surface energy and wettability.

In the present study, BSA- and DsRed-adsorption on the surface of thermally grown silica layers was investigated by changing the proteins concentrations. Silica is an amorphous material and the wettability properties of this thin layer with PPI water (same buffer solution used for the protein dilution) were investigated before starting the study on the protein adhesion. Given the measured advancing contact angle of $\theta_A = 63.2°$, this surface has hydrophilic properties. Moreover, when immersed in water, silica surfaces are known to acquire a negative surface charge density [50, 51]. The surface roughness was measured by cross sectional transmission electron microscopy and AFM studies. A value of 1.0 nm has been found, i.e. much smaller than the values reported for nano-TiO_2 [49]. Therefore, the effects on the conformation of proteins (such as structural transformation or protein denaturation) after their interaction with the surface depend also on the proteins charge status and, thus, on the pH-value of the proteins-containing solutions.

Despite the fact that the SE is a widely valid technique to estimate the thickness and the complex refractive index of even sub-nano layers, when biological targets are addressed or biological processes are discussed, it is sufficient and more straightforward to determine the surface concentration Γ, i.e. the adsorbed protein mass per unit area (μg cm^{-2}). If the layer is assumed to be transparent and the ellipsometric data allow both thickness and refractive index to be determined, one can

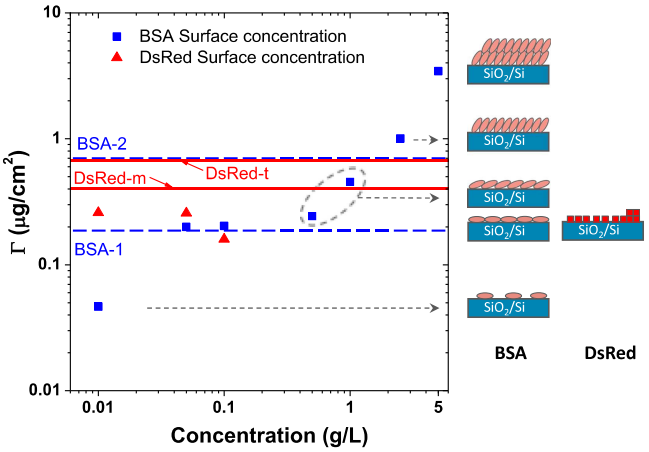


Figure 10. Surface concentration of the adsorbed BSA and DsRed protein layer on silica, calculated using the de Feijter's formula [36]. On the right side, schematics representing the scenario of thin layer formation for different proteins concentrations are reported.

use de Feijter's formula [36]:

$$\Gamma = \frac{d_p(n_p - n_0)}{\left(\frac{dn_p}{dc}\right)}, \tag{4}$$

where n_0 is the refractive index of the ambient and dn_p/dc is the refractive index increment for the molecules in the layer. In the literature, the refractive index increment for the molecules in the layer (dn_p/dc) is generally assumed to be around 0.18–0.19 $cm^3\,g^{-1}$ [52]. For BSA it was evaluated to 0.187 $cm^3\,g^{-1}$ [36]. The values of Γ for both BSA and DsRed thin protein layers, as determined in the current work, are reported in table 1 and represented on figure 10 in a log–log scale as a function of the protein concentration. According to previous BSA adsorption studies [1], the Γ-value and the protein layer thickness (d_p) can be used to understand the conformation of the proteins after dehydration: d_p-values of 4 nm describe BSA proteins adsorbed in 'side-on' configuration, i.e. with their major axis parallel to the surface, while d_p-values between 4 and 14 nm correspond to BSA proteins adsorbed 'end-on', i.e. with their major axis perpendicular to the surface. The d_p-value of 3.1 ± 0.2 nm, corresponding to the BSA layer obtained with lowest BSA concentration (0.01 $g\,l^{-1}$), shows a small difference in the layer thickness which can be explained by different extent of spreading of the protein molecules due to the fact that BSA is a soft protein and easily undergoes partial or total denaturation upon adsorption [1, 53, 54]. Another explanation, more reasonable in our opinion, is that the d_p-values extracted from SE measurements are actually equivalent thicknesses comprising of empty protein regions in the resulting protein layers.

The Γ-value of a protein mono-layer can be calculated for the two possible protein configurations taking into account the molecular weight of the BSA protein (66 kDa) and the surface occupied by one protein (4 × 14 nm^2 for 'side-on' and 4 × 4 nm^2 for 'end-on' configurations, respectively). Γ-values of 0.19 $\mu g\,cm^{-2}$ for no-spread 'side-on' and ~0.70 $\mu g\,cm^{-2}$ for no-spread 'end-on' protein mono-layer have been calculated in accordance with the literature [1, 33, 55–57]. The calculated Γ-values are reported in figure 10 as lines (indicated as BSA-1 and BSA-2, for 'side-on' and 'end-on' configurations, respectively), in comparison with the experimentally obtained ones (symbols). For the smallest investigated concentration, 0.01 $g\,l^{-1}$, the reported equivalent thickness is of 3.1 ± 0.2 nm. This value is compatible with the 'side-on' configuration. Both the equivalent thickness and the obtained Γ-value are smaller than the expected ones for a saturated mono-layer, suggesting that the BSA protein layer starts to form with proteins lying with their major axis parallel to the surface, although the surface coverage remains limited, of only 25% (see the suggested sketch in figure 10 for this concentration). As soon as the concentration is increased (0.05–0.1 $g\,l^{-1}$), the experimentally obtained Γ-values and the protein layer thicknesses reach the expected values for a saturated BSA layer in 'side-on' configuration, thus suggesting an evolution of the protein layer towards a more compact and uniform configuration (corresponding sketch in figure 10). The obtained higher values for the refractive index confirm the densification of these layers (figure 6). Further increase of the protein concentration in solution (0.5 and 1.0 $g\,l^{-1}$) results in thicker layers, higher refractive indexes and, finally, in higher surface densities Γ. In particular, for 1.0 $g\,l^{-1}$, both thickness of 5.3 nm and surface density of 0.46 $\mu g\,cm^{-2}$ suggest compact protein layer with proteins starting to deviate from the 'side-on' configuration, indicating reorientation of the major axis at tilted angle with respect to the SiO_2 surface (see corresponding sketch in figure 10). Starting from 2.5 $g\,l^{-1}$ the higher values of thickness and surface density can be explained by BSA protein adsorption in the 'end-on' configuration. For the highest investigated concentration of 5.0 $g\,l^{-1}$ the experimentally obtained thickness of 26.8 nm and the related Γ = 3.43 $\mu g\,cm^{-2}$ suggest formation of double or more complex compact layer structure (see corresponding sketch in figure 10). The higher refractive index (n_p = 1.56), found for BSA concentration of 5.0 $g\,l^{-1}$, supports this hypothesis in accordance with previously reported studies [1, 58].

The changes in the advancing contact angles by increasing the BSA concentration in the solution can be further correlated to the morphological changes of the protein layers and thus to be linked to their equivalent thickness (figure 9(b)). The increase of the advancing contact angles for d_p between 3.0–5.0 nm (i.e. between 0.01–0.5 $g\,l^{-1}$) suggests formation of a denser protein layer with more hydrophobic properties in accordance with the increased refractive index. Well expressed hydrophobic properties are reached for the BSA layer thickness of 6.0 nm (i.e. 1.0 $g\,l^{-1}$). Starting from this value on, for thicker protein layers a plateau is reached, owing to the fact that no further conformational changes occur in the layer density.

As far as the DsRed is concerned, considering its tetrameric structure in solution with a weight of 120 kDa where all monomers are packed together to form cubic-like shape, a surface area of 29.16 nm^2 is evaluated. Thus, for a saturated protein mono-layer constituted by tetramers, the expected surface concentration is Γ = 0.68 $\mu g\,cm^{-2}$ (DsRed-t line on figure 10). Given the monomer size, the surface area of the DsRed monomer is 11.56 nm^2. The Γ-value for a saturated

protein mono-layer constituted only by DsRed monomers is then 0.4 $\mu g\,cm^{-2}$ (DsRed-m line on figure 10). The experimentally obtained Γ-values for DsRed protein layers after adsorption and dehydration on the silica surface lay down in the range between 0.16–0.26 $\mu g\,cm^{-2}$, thus always smaller than the expected calculated ones, regardless the DsRed form —monomer or tetramer. They correspond at maximum to surface coverage between 40%–65% (corresponding sketch in figure 10). The obtained from SE equivalent protein layer thicknesses range between 3.7 and 4.2 nm which is rather compatible with the monomer size. This suggests structural rearrangements of the DsRed proteins when passing from planktonic state in solution to adsorption state when interacting with the solid silica surface. These interaction-induced changes lead to separation of the DsRed tetramer in monomers, although some residual tetramers result in equivalent layer thickness larger than the DsRed monomer size ($d_p = 4.2$ nm for $0.05\,g\,l^{-1}$ as shown in the sketch in figure 10, in agreement with the AFM PF-QNM height histogram in figure 2(f)). The obtained results therefore suggest the presence of a non-continuous layer on the silica surface for all the investigated concentrations and morphology state in accordance with the AFM PF-QNM-measurements where a rod-like structure was identified. Moreover, as reported previously, proteins with strong internal coherence do not adsorb easily on hydrophilic surfaces [11, 17, 18]. These last evidences, combined with the presence of the DsRed typical absorption peaks in the IR spectrum of the protein, reported in figure 4(a), and the strong red PL signal, reported in figure 4(b), further confirm the absence of denaturation (unfolding) after dehydration on the silica surface, in accordance with a previous study [45].

Although the investigated DsRed concentrations match some of the BSA ones, they remain small to achieve continuous mono-layer. Moreover the mechanisms of the thin layer organization largely differ for the two studied proteins. Complete mono-layer was achieved only for the BSA proteins. This evidence can be explained by considering both the different protein size and the solution pH-value, compared to the protein isoelectric points (pH-value at which the proteins carry no net electrical charge). Indeed, a saturated BSA mono-layer in 'side-on' configuration contains 1.7×10^{12} proteins cm^{-2}, while for a DsRed mono-layer constituted by monomers this value reaches 8.6×10^{12} proteins cm^{-2}, which is five times higher. The pH-values of BSA and DsRed solutions have been measured to 5.6 and 6.6, respectively. For BSA, this value is very close to the protein isoelectric points, thus having only a small negative charge; large variations from the isoelectric points are indeed well known to alter the BSA secondary structure [59, 60]. Therefore, one can expect that the adhesion process of BSA proteins on the hydrophilic and negatively charged silica layer is optimized under these conditions. It is mainly driven by the van der Waals or the induced dipole forces with repulsion of only a small fraction of proteins, due to their slightly negative charges in accordance with the adsorption studies on other hydrophilic surfaces, such as GeOH [19]. Concerning DsRed, its secondary structure has been found to remain very stable for a large variation of the pH-values. Almost no changes are observable in the 4–11 pH-range [45, 61, 62]. The higher measured pH-value of DsRed solution (6.6) compared to the one of BSA solution (5.6) suggests that the proteins are negatively charged and therefore the rate at which they interact with the surface is strongly attenuated owing to the occurrence of a significant electrostatic repulsion before adsorption [60]. Given also the DsRed strong internal coherence, the protein adsorption on silica surfaces is reduced under the above conditions although separation in monomers is achieved.

These results demonstrate the importance to evaluate protein adhesion to bioactivated surfaces. This opens new perspectives for building up a more realistic scenario representing plasma proteins in intermixed proteins/proteins systems, micro-organisms and more complex organizations, such as proteins/micro-organisms hybrid systems. The substantial role played by the competitive adsorption of different plasma proteins has to be considered [49, 63] in addition to the already discussed influencing factors related to the surface properties. This requires further studies by weighting the contribution of each constituent to the 'protein-adsorption problem'.

6. Conclusions

In this work we have investigated the adsorption process of BSA (optically non-absorbing, model protein) and DsRed (optically absorbing, naturally fluorescent protein) on silica surfaces, their organization in thin layers and their state after dehydration. Uniform protein thin layers on silica were processed by dip coating. The evolution of the layer thickness by changing the protein concentration was followed *ex situ* by SE evidencing the dynamics of the formation of the thin layers. The possibility to finely control the proteins layer thickness by properly tuning the solutions' concentration is demonstrated. Specifically, the small thickness, the low refractive index and the small surface coverage measured for the lowest BSA concentration ($0.01\,g\,l^{-1}$) suggest the presence of a non-continuous and non-dense mono-layer that evolves towards (i) a compact mono-layer for intermediate concentrations ($0.05–1.0\,g\,l^{-1}$) and (ii) a complex structure for higher concentration ($>1.0\,g\,l^{-1}$). Concerning DsRed, only non-continuous mono-layers mainly constituted by monomers (surface coverage between 40%–65%) were obtained for all the investigated concentrations. Even though structural rearrangement leading to separation of the DsRed tetramers into monomers occurs after interaction with solid silica surfaces, some residual tetramers are observed. The thicknesses extracted from SE measurements and analysis, were confirmed by AFM PF-QNM analyses. These differences in the BSA and DsRed thin layers formation are due to the smaller DsRed dimensions compared to those of BSA, which result in a much higher required number of proteins (five times larger) needed to obtain a saturated DsRed mono-layer. Regarding the internal coherence and the isoelectric points of the two proteins a reduced adsorption was found for the DsRed compared to the BSA. Besides, different protein

organizations on the silica surface are observed being a lace-like network for the BSA and a rod-like structure for the DsRed. By bringing together the information obtained by FTIR (presence of the Amide I and II bands for both proteins thin layers) and PL measurements (presence of an intense red emission for the DsRed thin layers), we can exclude protein unfolding and denaturation and suggest the preservation of the proteins' secondary structure after dehydration. Therefore, these results reveal the advantage of the proposed synthesis process to realize uniform, non-denaturated thin proteins layers with controlled thicknesses down to mono-layer level (<5 nm) thus opening the possibility to apply the proposed methods for more complex organizations, such as intermixed proteins/proteins and proteins/micro-organisms systems.

Acknowledgments

This work is financially supported by the program IDEX Transversalité of Université de Toulouse (ANR-11-IDEX-0002-02), under project ADAGIO and the project ND-AgNPs of CNRS MI Inter-Instituts. M S acknowledges the PhD-grant from Université de Toulouse—Région Occitanie, Toulouse, under APR project ADAGIO.

ORCID iDs

A Scarangella https://orcid.org/0000-0001-8645-7770
C Villeneuve-Faure https://orcid.org/0000-0002-7959-2912
C Bonafos https://orcid.org/0000-0001-5140-6690
K Makasheva https://orcid.org/0000-0001-6113-3593

References

[1] Silva-Bermudez P, Rodila S E and Muhla S 2011 Albumin adsorption on oxide thin films studied by spectroscopic ellipsometry *Appl. Surf. Sci.* **258** 1711–8
[2] Eisenbarth E, Velten D and Breme J 2007 Biomimetic implant coatings *Biomol. Eng.* **24** 27–32
[3] Ochsenbein A, Chai F, Winter S, Traisnel M, Breme J and Hildebrand H F 2008 Osteoblast responses to different oxide coatings produced by the sol–gel process on titanium substrates *Acta Biomater.* **4** 1506–17
[4] Birge R R *et al* 1999 Biomolecular electronics: protein-based associative processors and volumetric memories *J. Phys. Chem.* B **103** 10746–66
[5] Senveli S U and Tigli O 2013 Biosensors in the small scale: methods and technology trends *IET Nanobiotechnol.* **7** 7–21
[6] Parlak O and Turner A P F 2016 Switchable bioelectronics *Biosens. Bioelectron.* **76** 251–65
[7] Tamerler C, Khatayevich D, Gungormus M, Kacar T, Oren E E, Hnilova M and Sarikaya M 2010 Molecular biomimetics: GEPI-based biological routes to technology *Biopolymers* **94** 78–94
[8] Wilson C J, Clegg R E, Leavesley D I and Pearcy M J 2005 Mediation of biomaterial–cell interactions by adsorbed proteins: a review *Tissue Eng.* **11** 1–18
[9] Werner C, Maitz M F and Sperling C 2007 Current strategies towards hemocompatible coatings *J. Mater. Chem.* **17** 3376–84
[10] Parhi P, Golas A and Vogler E A 2010 Role of proteins and water in the initial attachment of mammalian cells to biomedical surfaces: a review *J. Adhes. Sci. Technol.* **24** 853–88
[11] Vogler E A 2012 Protein adsorption in three dimensions *Biomaterials* **33** 1201–37
[12] Roach P, Farrar D and Perry C C 2005 Interpretation of protein adsorption: surface-induced conformational changes *J. Am. Chem. Soc.* **127** 8168–73
[13] Valencia-Serna J, Chevallier P, Bahadur K C R, Laroche G and Uludag H 2016 Fibronectin-modified surfaces for evaluating the influence of cell adhesion on sensitivity of leukemic cells to siRNA nanoparticles *Nanomedicine* **11** 1123–38
[14] Saulou C, Jamme F, Maranges C, Fourquaux I, Despax B, Raynaud P, Dumas P and Mercier-Bonin M 2010 Synchrotron FTIR microspectroscopy of the yeast *Saccharomyces cerevisiae* after exposure to plasma-deposited nanosilver-containing coating *Anal. Bioanal. Chem.* **396** 1441–50
[15] Mercier-Bonin M, Duviau M-P, Ellero C, Lebleu N, Raynaud P, Despax B and Schmitz P 2012 Dynamics of detachment of *Escherichia coli* from plasma-mediated coatings under shear flow *Biofouling* **28** 881–94
[16] Norde W 2008 My voyage of discovery to proteins in flatland… and beyond *Colloids Surf.* B **61** 1–9
[17] Arai T and Norde W 1990 The behavior of some model proteins at solid–liquid interfaces 1. Adsorption from single protein solutions *Colloids Surf.* **51** 1–15
[18] Norde W and Anusiem A C I 1992 Adsorption, desorption and re-adsorption of proteins on solid surfaces colloid and surfaces *Colloids Surf.* **66** 73–80
[19] Jeyachandran Y L, Mielczarski E, Rai B and Mielczarski J A 2009 Quantitative and qualitative evaluation of adsorption/desorption of bovine serum albumin on hydrophilic and hydrophobic surfaces *Langmuir* **25** 11614–20
[20] Cross M C, Toomey R G and Gallant N D 2016 Protein-surface interactions on stimuli-responsive polymeric biomaterials *Biomed. Mater.* **11** 022002
[21] Lacy W B, Williams J M, Wenzler L A, Beebe T P Jr and Harris J M 1999 Characterization of SiO_2-overcoated silver-island films as substrates for surface-enhanced raman scattering *Anal. Chem.* **68** 1003–11
[22] Carles R, Farcau C, Bonafos C, BenAssayag G, Bayle M, Benzo P, Groenen J and Zwick A 2011 Three dimensional design of silver nanoparticle assemblies embedded in dielectrics for raman spectroscopy enhancement and dark-field imaging *ACS Nano* **5** 8774–82
[23] Pugliara A, Bonafos C, Carles R, Despax B and Makasheva K 2015 Controlled elaboration of large-area plasmonic substrates by plasma process *Mater. Res. Express* **2** 065005
[24] Irene E A 1985 Silicon oxidation *Integrated Circuits: Chemical and Physical Processing* ed P Stroeve vol 290 (Washington, DC: American Chemical Society) ch 3 pp 31–46
[25] Blomback B and Hanson L A 1976 *Plasma Proteins* (New York: Wiley)
[26] Peters T Jr 1996 All about albumin: biochemistry *Genetics and Medical Applications* (New York: Academic)
[27] Matz M V, Fradkov A F, Labas Y A, Savitsky A P, Zaraisky A G, Markelov M L and Lukyanov S A 1999 Fluorescent proteins from nonbioluminescent anthozoa species *Nat. Biotechnol.* **17** 969–73
[28] El Khatib M, Martins A, Bourgeois D, Colletier J-P and Adam V 2016 Rational design of ultrastable and reversibly photoswitchable fluorescent proteins for superresolution imaging of the bacterial periplasm *Sci. Rep.* **6** 18459

[29] European Directorate for the Quality of Medicines 2008 *European Pharmacopoeia: Supplement 6.3* 6th edn (Strasbourg: Council of Europe)

[30] Yarbrough D, Wachter R M, Kallio K, Matz M V and Remington S J 2001 Refined crystal structure of DsRed, a red fluorescent protein from coral, at 2.0 Å resolution *Proc. Natl Acad. Sci.* **98** 462–7

[31] SEMILAB 2017 Spectroscopic Ellipsometry Analyser—SEA (WinElli 3) version 1.5.50

[32] Bevington P R 1969 *Data Reduction and Error Analysis for the Physical Sciences* (New York: McGraw-Hill)

[33] Arwin H 2014 Adsorption of proteins at solid surfaces *Ellipsometry of Functional Organic Surfaces and Films* (Berlin: Springer)

[34] Mora M F, Wehmeyer J L, Synowicki R and Garcia C D 2009 Investigating protein adsorption via spectroscopic ellipsometry *Biological Interactions on Materials Surfaces: Understanding and Controlling Protein, Cell, and Tissue Responses* ed D A Puleo and R Bizios (Berlin: Springer)

[35] Arwin H 2001 Is ellipsometry suitable for sensor applications? *Sensors Actuators* A **92** 43–51

[36] de Feijter J A, Benjamins J A and Veer F A 1978 Ellipsometry as a tool to study the adsorption behaviour of synthetic and biopolymers at the air–water interface *Biopolymers* **17** 1759–72

[37] Spaeth K, Brecht A and Gauglitz G 1997 Studies on the biotin-avidin multilayer adsorption by spectroscopic ellipsometry *J. Colloid Interface Sci.* **196** 128–35

[38] Poksinski M and Arwin H 2004 Protein monolayers monitored by internal reflection ellipsometry *Thin Solid Films* **455–456** 716–21

[39] Karlsson L M, Schubert M, Ashkenov N and Arwin H 2004 Protein adsorption in porous silicon gradients monitored by spatially-resolved spectroscopic ellipsometry *Thin Solid Films* **455–456** 726–30

[40] Berlind T, Tengvall P, Hultman L and Arwin H 2011 Protein adsorption on thin films of carbon and carbon nitride monitored with *in situ* ellipsometry *Acta Biomater.* **7** 1369–78

[41] Synowicki R A, Pribil G K, Cooney G, Herzinger C M, Green S E, French R H, Yang M K, Burnett J H and Kaplan S 2004 Fluid refractive index measurements using rough surface and prism minimum deviation techniques *J. Vac. Sci. Technol.* B **22** 3450–3

[42] Nejadnik M R and Garcia C D 2011 Staining proteins: a simple method to increase the sensitivity of ellipsometric measurements in adsorption studies *Colloids Surf.* B **82** 253–7

[43] Lousinian S, Logothetidis S, Laskarakis A and Gioti M 2007 Haemocompatibility of amorphous hydrogenated carbon thin films, optical properties and adsorption mechanisms of blood plasma proteins *Biomol. Eng.* **24** 107–12

[44] Marchant J S, Stutzmann G E, Leissring M A, LaFerla F M and Parker I 2001 Multiphoton-evoked color change of DsRed as an optical highlighter for cellular and subcellular labeling *Nat. Biotechnol.* **19** 645–9

[45] Soumbo M, Pugliara A, Monje M-C, Roques C, Despax B, Bonafos C, Carles R, Mlayah A and Makasheva K 2016 Physico–chemical characterization of the interaction of red fluorescent protein-DsRed with thin silica layers *IEEE Trans. NanoBiosci.* **15** 412–7

[46] Kirk C T 1988 Quantitative analysis of the effect of disorder-induced mode coupling on infrared absorption in silica *Phys. Rev.* B **38** 1255–73

[47] Barth A 2007 Infrared spectroscopy of proteins *Biochim. Biophys. Acta* **1767** 1073–101

[48] Khalilzadeh P, Lajoie B, El Hage S, Furiga A, Baziard G, Berge M and Roques C 2010 Growth inhibition of adherent *Pseudomonas aeruginosa* by an *N*-butanoyl-l-homoserine lactone analog *Can. J. Microbiol.* **56** 317–25

[49] Lorenzetti M, Bernardini G, Luxbacher T, Santucci A, Kobe S and Novak S 2015 Surface properties of nanocrystalline TiO_2 coatings in relation to the *in vitro* plasma protein adsorption *Biomed. Mater.* **10** 045012

[50] Behrens S H and Grier D 2001 Electrostatic interaction of colloidal surfaces with variable charge *J. Phys. Chem.* **115** 6716

[51] Kokot G, Bespalova M I and Krishnan M 2016 Measured electrical charge of SiO_2 in polar and nonpolar media *J. Chem. Phys.* **145** 194701

[52] Puleo D A and Bizios R 2009 *Biological Interactions on Materials Surfaces: Understanding and Controlling Protein, Cell, and Tissue Responses* (Berlin: Springer)

[53] Haynes C A and Norde W 1995 Structures and stabilities of adsorbed proteins *J. Colloid Interface Sci.* **169** 313–28

[54] Norde W and Giacomelli C E 1999 Conformational changes in proteins at interfaces: from solution to the interface, and back *Macromol. Symp.* **145** 125–36

[55] McClellan S J and Franses E I 2003 Effect of concentration and denaturation on adsorption and surface tension of bovine serum albumin *Colloids Surf.* B **28** 63–75

[56] Byrne T M, Lohstreter L B, Filiaggi M J, Bai Z J and Dahn J R 2009 Quantifying protein adsorption on combinatorially sputtered Al-, Nb-, Ta- and Ti-containing films with electron microprobe and spectroscopic ellipsometry *Surf. Sci.* **603** 992–1001

[57] Maleki M S, Moradi O and Tahmasebi S 2017 Adsorption of albumin by gold nanoparticles: Equilibrium and thermodynamics studies *Arab. J. Chem.* **10** S491–502

[58] Benesch J, Askendal A and Tengvall P 2002 The determination of thickness and surface mass density of mesothick immunoprecipitate layers by null ellipsometry and protein ^{125}iodine labeling *J. Colloid Interface Sci.* **249** 84–90

[59] Peters T Jr 1985 Serum albumin *Adv. Protein Chem.* **37** 161–245

[60] Freeman N J, Peel L L, Swann M J, Cross G H, Reeves A, Brand S and Lu J R 2004 Real time, high resolution studies of protein adsorption and structure at the solid–liquid interface using dual polarization interferometry *J. Phys.: Condens. Matter* **16** S2493–6

[61] Baird G S, Zacharias D A and Tsien R Y 2000 Biochemistry, mutagenesis, and oligomerization of DsRed, a red fluorescent protein from coral *Proc. Natl Acad. Sci.* **97** 11984–9

[62] Vrzheshch P V, Akovbian N A, Varfolomeyev S D and Verkhusha V V 2000 Denaturation and partial renaturation of a tightly tetramerized DsRed protein under mildly acidic conditions *FEBS Lett.* **487** 203–8

[63] Magnani A, Barbucci R, Lamponi S, Chiumento A, Paffetti A, Trabalzini L, Martelli P and Santucci A 2004 Two-step elution of human serum proteins from different glass-modified bioactive surfaces: a comparative proteomic analysis of adsorption patterns *Electrophoresis* **25** 2413–24